Oxygenate formation over K/β-Mo_2C catalysts in the Fischer-Tropsch synthesis

Wijnand Marquart, [a] David J. Morgan, [b] Graham J. Hutchings,[b] Michael Claeys[a] and Nico Fischer[a]

The Fischer-Tropsch (FT) process, producing long chained waxes and transportation fuels, is competing with fuels derived from crude oils and its profitability is therefore dependent on the global oil price. However, increasing the value of synthesized products could render the profitability of the FTS independent of the common fluctuations in the commodity price (which are mostly due to global political trends and only to a lesser extent due to market requirements). One way to achieve this, is to target the more valuable products of the Fischer-Tropsch spectrum, for example oxygenates. This study investigates effect of synthesis protocols on the surface characteristics of molybdenum carbide and the use of potassium promoted Mo_2C as a catalyst for higher oxygenate (C_{2+} oxygenates) synthesis in CO hydrogenation. A graphitic surface layer was observed with TEM, XPS and Raman analysis for Mo_2C samples carburized at ≥760 °C. The graphitic carbon, blocking active sites and therefore significantly lowering catalytic activity, could be partially removed by means of a temperature programmed hydrogenation, forming methane. An unpromoted β-Mo_2C catalyst, carburized at 630°C, reached CO conversions up to ±40% at the conditions applied. Initial 6.2 wt.% K/Mo promotion of the catalyst with potassium showed a significant drop in catalyst activity, however, an increase in potassium content did not further decrease catalyst activity. The selectivity towards oxygenates was enhanced, yet it has a certain optimum with regards to promotor concentration. Simultaneously, the oxygenate distribution shifted towards higher alcohols. The initial methanol content in the total oxygenate product was around 60 C% and decreased to approximately 20 C% upon potassium promotion.

1. Introduction

The Fischer-Tropsch synthesis (FTS) can be described as the formation of hydrocarbons (paraffins and olefins) as well as oxygenates (alcohols, aldehydes, ketones and carboxylic acids) and water through a catalytic surface polymerization reaction of synthesis gas (combination of CO and H_2) [1-6]. A commercial FT-plant includes three main process steps. The preparation of the synthesis gas from coal, biomass or natural gas (methane) via steam/autothermal reforming or gasification processes being the first stage. The produced syngas is converted into products such as paraffins, olefins, water and, to a certain extent, oxygenates via an exothermic surface polymerization reaction over transition metal catalysts. As the reaction produces a mixture of different product slates extensive downstream processing is required to increase the yield of fuels, waxes and other chemicals.

Besides producing transportation fuels, the profitability of which is mostly dependent on fluctuations of the global crude oil price, the product spectrum derived from the FTS process can also be altered towards more valuable chemicals [6]. Typical albeit minor products, such as oxygenates can further be processed to produce a range of high value products. The profitability of the FTS process is therefore less dependent on the global crude oil price.

Producing long chained oxygenates (e.g. higher alcohol synthesis) at high selectivity, has been in the focus of researchers for many years, especially in the context of cleaner gasoline. Vehicle gasoline engines require a certain octane number (ON), which is the volumetric percentage of iso-octane in the gasoline. To put it in perspective, pure iso-octane has an ON of 100 and *n*-heptane an ON of 0. A high-octane number in the gasoline (usually ON of 93-97) prevents its engine from ''knocking'' (premature burning of the fuel in the combustion chamber causing a small explosion in the engine before the piston has achieved full compression). Initially, the increase of the octane number was achieved by adding lead containing compounds such as tetraethyl lead to the gasoline [7]. However, the environmental protection agency (EPA) called for reducing lead concentrations in gasoline as lead was identified as a pollutant and poison. Nowadays, the octane number in gasoline can be increased by addition of aromatic hydrocarbons or oxygenates. The use of aromatics produces more particulates, smog, and it increases the released benzene to the atmosphere, which is known as a carcinogenic compound [8]. Methyl tert-butyl ether (MTBE) is also known to increase the ON, however, the addition of MTBE has shown to contaminate water resources mainly via leaking storage tanks, pipelines, refuelling spills and emissions from older marine engines [9]. Oxygenates added to the gasoline help to combust the fuel to a higher degree due to the additional presence of oxygen. Therefore, it increases the efficiency of the combustion process and reduces the emission of pollutants into the air. Pure ethanol has an octane number of over 100, thus 84 octane gasoline can be blended with 10 percent ethanol to reach the minimum requirement ON of 87 for retail gasoline in the United States [9, 10].

[a] *Catalysis Institute and c*change (DST-NRF Centre of Excellence in Catalysis), Department of Chemical Engineering, University of Cape Town, Rondebosch 7701, Cape Town, South Africa.*
[b] *Cardiff Catalysis Institute, School of Chemistry, Cardiff University, Main Building, Park Place, CF10 3AT, United Kingdom.*

Typically, transition metals such as Fe, Co, Rh and Ni are active for the FT synthesis. Based on reaction conditions employed, commercial Fe and Co based catalysts have been shown to produce between 6 and 12% oxygenates [11]. The Institut Français du Pétrole (IFP) patented the production of a mixture of methanol and higher alcohols using copper-cobalt-alloy catalysts [12]. These IFP-catalysts have shown high selectivity towards higher alcohols, with a very low amount of methanol produced. However, the catalysts have shown to have low activity due to the suppression of hydrocarbon formation and show significant deactivation with time on stream [13]. Fe-based catalysts targeting oxygenates in the FT synthesis were investigated by numerous authors. Based on studies which suggested that the oxidic phase of the iron catalysts is responsible for the formation of oxygenates Zhang *et al.* (2010) [14] studied Fe_2O_3/Al_2O_3 catalysts in a CSTR at reaction conditions of 30 bar and 250°C [15, 16]. At approximately 12% CO conversion a weight ratio of oxygenated compounds to hydrocarbons of 95/5 was achieved. Rh has been shown to have a high oxygenate selectivity, but the associated high raw material cost becomes prohibitive for use as a commercial FT catalyst [17]. Transition metal carbides/nitrides or oxycarbides have shown promising results and high activity for CO hydrogenation [18]. Mo_2C has also been shown to be resistant to sulphur poisoning (which is a typical impurity in synthesis gas especially when derived from coal). Previous investigations using Mo-based catalysts for CO hydrogenation towards higher alcohols are mostly focused on the sulfide, carbide or nitride form [17, 19-21].

Two different crystal structures of molybdenum carbide (β-Mo_2C, hcp, and α-MoC_{1-x}, fcc) were compared by Xiang *et al.* (2006) [22], in the presence of different amounts of K_2CO_3. Overall, the hcp-crystal structure of molybdenum carbide showed a higher oxygenate selectivity and chain growth than the fcc-crystal structure.

Xiang *et al.* (2008) [21] studied four potassium promoted β-Mo2C catalysts, with three of them also being promoted with Co, Ni or Fe. The Fe/K-, Co/K- and Ni/K-promoted catalysts show a decrease in the formation of C_1 and C_2 alcohols, but an increase in the formation of C_{3+} alcohols, specifically butanol, compared to the K-promoted catalyst.

Wu *et al.* (2013) [23] studied the effect of β-Mo2C-based catalysts on high surface area support materials. Comparing to the potassium promoted bulk carbide, TiO2 showed the only increase in selectivity to higher alcohols (from ~30% to ~35% at 250°C), but the selectivity towards hydrocarbons remained similar (~50% to ~47% at 250°C). The high surface area phase of TiO_2, anatase, transformed (>550°C) to the low surface area phase, rutile, during the high temperature carburization (750°C).

This study will therefore focus on the synthesis of a β-Mo_2C catalyst, promoted with different levels of potassium, and its Fischer-Tropsch synthesis performance evaluated in a stainless steel fixed bed reactor. The influence of catalyst synthesis protocols (specifically regarding the observed carbon depositions on the catalyst surface by Mo *et al.* (2016) [24] at high carburization temperatures), reactor pressure and temperature, feed gas space velocity, and K/Mo wt.% promotion on catalyst activity and selectivity were investigated.

2. Experimental

Catalyst preparation

The preparation of a hexagonal molybdenum carbide (β-Mo_2C) catalyst is based on the method reported by Lee *et al.* (1987) [25]. The conditions for the temperature programmed reaction of MoO_3 with a 20% CH_4/H_2 mixture were varied to be able to observe its influence on the characteristics of the catalyst and its performance in the Fischer-Tropsch synthesis. All samples prepared for catalyst evaluation were obtained by heating ammonium molybdate ($(NH_4)_6Mo_7O_{24}{\cdot}4H_2O$, >81.5%, SAARCHEM PTY LTD) in a calcination oven (Nabertherm, LT 5/12) in an air atmosphere. Samples were placed into a ceramic crucible and heated to 500°C at a heating rate of 10°C/min holding for 5 h [26-28]. Subsequently, the oven was set to cool down to room temperature. The sample was removed from the oven and crushed using a mortar and pestle to a fraction of below 200 µm. The hexagonal phase of β-Mo_2C was formed by slowly heating the oxide precursor, MoO_3, in a gaseous mixture of 20% CH_4 in H_2 (AFROX). The reaction was performed, by placing 2-3 gram of the oxide precursor in a double walled quartz tube (15 mm i.d,) inside a tubular furnace (Elite TSV12/38/250). All FT-tested catalysts were prepared by an *in situ* carburization method. Instead of a quartz tube, a ¼" stainless-steel U-tube reactor was employed and the total mass of the MoO_3 precursor was decreased to ±1 g.

In general, the final carburization temperature was set between 630 and 1000°C with heating rates varying between 1-10°C/min up to a temperature of 400/450°C (as no reaction occurs up to ±450°C [25]). A heating rate of 1-2°C/min was set from 400/450°C onwards to the final carburization temperature, holding the final temperature for between 2 to 5 h. At temperatures of ≥ 760°C, carbon deposition in the form of graphite is expected [24].

After the carburization reaction, the catalyst was cooled to room temperature. Before the catalyst was exposed to air, the catalyst undergoes a post-treatment passivation with 50 $ml/min/g_{cat}$ of 1% O_2 in N_2 (AFROX) for 1 h at room temperature. In general, the passivation step is completed for all catalysts, prepared in the quartz tube and stainless-steel U-tube, as it is required for offline catalyst characterization and subsequent promotion. However, an *in situ* sample was prepared, therefore not passivated before being exposed to testing conditions, to study the passivation effect on the activity and selectivity of the catalyst.

The preparation of the promoted samples was achieved by a wetness impregnation method. The addition of potassium was based on a K/Mo ratio of 2.5 wt.%, 5.0 wt.% and 7.5 wt.%. Potassium carbonate (K_2CO_3, SAARCHEM) was dissolved in a few drops of distilled water, until a clear solution was obtained. Subsequently, the β-Mo_2C sample was added to the K_2CO_3-

solution while stirring slowly, forming a smooth suspension. Once mixed properly, the suspension was dried in a drying oven for 1 to 2 h at 120°C. The dried sample was then calcined at 500°C for 2 h at a heating rate of 5°C/min under 50 ml/min/g_{cat} of argon [22].

Catalyst characterization

X-ray diffraction (XRD) measurements were used to analyse the crystalline phases of the components of the catalysts. The obtained diffraction patterns were compared with reference data files reported in a database (ICDD PDF_2). The analysis was carried out in a D8 Advance Bruker laboratory X-ray diffractometer operated at 35 kV and 40 mA with a cobalt source (λ = 1.78897 Å) and position sensitive detector (LynxEye E 1D mode). The scan range was set from 20° to 120° 2Θ, with a step size of 0.043° and a time per step of 0.75s. Total scan time was 29 min and 50 s.

Transmission electron microscopic (TEM) images of the prepared catalysts were taken with a Tecnai F20 transmission electron microscope equipped with a field emission gun (operated at 200 kV).

X-ray photoelectron spectroscopy (XPS) was carried out to observe the elemental composition on the surface of the catalyst. The measurements were conducted in a Kratos Axis Ultra DLD photoelectron spectrometer utilizing Al radiation (1486.6 eV photon energy). All data was acquired at a pass energy of 40 eV for high resolution spectra and 160 eV for survey scans. Step size was 0.1 eV for high resolution scans and 1 eV for the survey scans. Charge compensation was achieved using the Kratos immersion lens system and all spectra subsequently calibrated to the C 1s line taken to be 284.8 eV. Data analysis was completed with the CasaXPS software (v2.3.17 PR1.1) applying sensitivity factors from the manufacturer.

Raman spectroscopy was performed to analyse the surface of the catalyst to observe any carbon deposition (graphitic/amorphous) and the presence of oxide layers, MoO_x, as these are strong Raman scatterers. The analysis was carried out with a Renishaw inVia Raman Microscope equipped with a green laser (532 nm). The software used for data analysis was WiRE 3.4 HF5925 build 2377. The measurements were completed setting the laser power between 20-60 MW to minimize sample heating.

Temperature programmed hydrogenation (TPH) experiments were performed studying the removal of the deposited carbon species, formed during the high temperatures of carburization, from the surface of the catalyst. The TPH experiment was completed by analysing the β-Mo_2C sample inside the calcination unit equipped with a GC-TCD (Varian CP-4900) to monitor the CH_4 formation. The sample was heated to 800°C under a hydrogen flow of ±150 ml/min/g_{cat} using a ramp rate of 1°C/min.

Inductively coupled plasma optical emission spectrometry (ICP-OES) measurements on the samples were conducted by means of a Varian OES 730 Series spectroscope. ICP-OES analysis was performed to determine the metal loadings of potassium as well as molybdenum content in the catalysts. The instrument was equipped with a radial torch configuration and scandium as an internal standard. This method can be used to quantify small traces of metals in the catalyst as it is highly sensitive. Sample preparation is completed by a typical acid digestion in HCl (3 ml), HF (3 ml) and a few droplets of HNO_3 in a reactor containing bi-distilled water. The process continued by heating the mixture to 130°C, stirring for 1 h and then cooling under a jet of water. Residue is avoided by the addition of H_3BO_3 (60 ml) while stirring. After filtration, the solution is injected into the spectroscope.

In situ powder X-ray diffraction measurements were performed in a XRK900 Anton Paar reaction cell attached to a laboratory XRD (Bruker D8 Advance) operated at 47 kV and 35 mA equipped with a molybdenum source (λ = 0.7107 Å) and a position sensitive detector (Bruker AXS Vantec). The samples were analysed with a scan range of 13° to 40° 2Θ with step size: 0.0287°. Time per step was 0.2s, and scan time 5.0 min. The obtained diffraction patterns were compared to reference patterns recorded in the ICDD PDF-2 database and analysed using Rietveld refinement techniques (TOPAS 4.1 software package, Bruker AXS).

Catalyst testing

The testing of the catalysts was performed in a lab scale ¼" stainless steel U-shaped fixed bed reactor. Prior to the Fischer-Tropsch experiments, the catalyst samples are treated in 50 ml/min/g_{cat} hydrogen at atmospheric pressure and 400°C with a ramp rate of 5°C/min for 4.5 h to reduce the catalyst and to remove the oxide layer formed during the passivation step. This pretreatment is commonly reported in literature [24, 29, 30]. Exception is made for one *in situ* prepared non-promoted catalyst, which was not passivated. Upon termination of the reaction, the argon flow is shut off and the catalyst was unloaded, without any post FT-run passivation method.

All selectivities towards CH_4 and CO_2 presented in the results section are calculated based on 'carbon balance corrected' selectivities to address the impact of the measurement error of the CO concentration in the reactor outlet gas, especially at low conversion conditions (<5%). Therefore, to ''correct'' the selectivities towards CO_2 and CH_4, they are divided by the carbon balance. Selectivities towards the other organic products are not affected as they are generally presented as ratios. This process is conducted for all results presented to maintain consistency (see Table S1 and S2 for details on product analysis and the gas chromatography conditions).

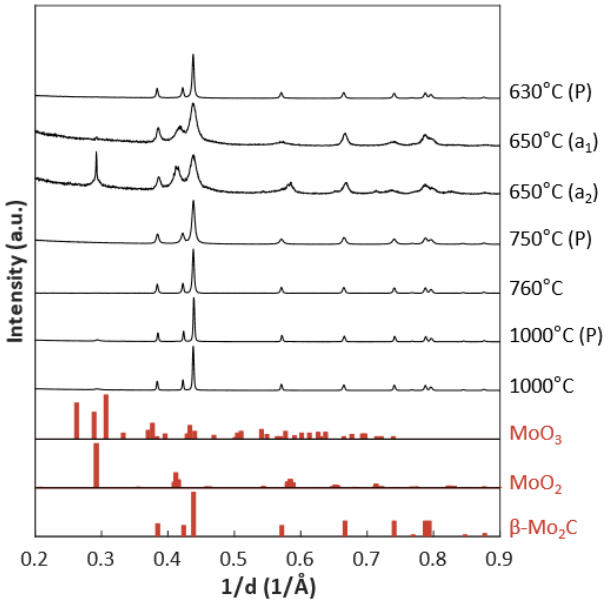

Fig. 1 XRD analysis of (passivated, P, and in situ XRD) samples prepared under different carburization temperatures. Reference patterns of molybdenum oxides and carbide shown in red.

3. Results and discussion

Characterization of catalysts not tested in the Fischer-Tropsch synthesis

Effect of carburization temperature. Three catalysts were prepared using 20% CH_4/H_2 in three different temperature zones, i.e. 630-650°C, 750-760°C and 1000°C at a heating rate of 0.5 to 1°C/min and a holding time of 2 to 5 h to observe the effect of the different carburization conditions on the phase composition of the catalyst. Of each condition one sample was passivated and one sample extracted directly for characterization to investigate the stability against oxidation in air. XRD-analysis was performed to determine the composition and the crystalline phase of the catalysts (Fig.).

After carburization at 630 and 650°C the sample re-oxidized if not passivated, shown by a sample prepared *in situ* in the XRD at 650°C and subsequently exposed to air (in Fig.: 650°C a_1 – freshly carburized and measured in the *in situ* XRD cell; 650°C a_2 – same sample measured after removal from the in situ XRD cell and exposure to air without passivation). MoO_2 was formed and exhibited a bimodal crystallite size distribution. The average crystallite sizes were determined using Rietveld refinement [31]. The large MoO_2 crystallite sizes (93.9±23.8 nm) are believed to be formed during the very high temperature of the sample upon exposure to air, i.e. the violent exothermic re-oxidation of the carbide phase, resulting in sintering of the catalyst particles. The small crystallite sized MoO_2 (9.9±0.9 nm) is identified as oxide fractions which did not entirely carburize in the first place. The average crystallite size of β-Mo_2C carburized sample at 630°C was 35.0±0.3 nm.

The samples prepared at 750 and 760°C, indicated that the passivation step is apparently not required anymore and that both samples are stable in air; at least with respect to their bulk crystal phases. The average crystallite sizes are different from one another (20.3 and 38.8 nm), which is possibly associated to the difference in holding time (2 and 5 h, respectively). The composition of the 1000°C sample was calculated, via full pattern Rietveld refinement, were to consist of 97 wt.% β-Mo_2C, with an average crystallite size of 63.6±0.6 nm, balanced by MoO_2 with a crystallite size of 12.7±1.4 nm. However, this is believed to be residual MoO_2 which is not carburized initially, rather than re-oxidized due to the small crystallite size of the MoO_2 phase. Again, passivation was not required to avoid bulk re-oxidation as observed for the 650°C samples.

Transmission electron microscopy (TEM) of the samples shows clear differences specifically on the edges of the particles (Fig.). The sample prepared at a carburization temperature of 630°C followed by passivation showed a dense clustered particle without any clear graphite deposition or oxide formation. With an increase in carburization temperature to 760°C, the formation of an unevenly distributed layer of a few nm thickness is observed. The thickness of the layer increases with increasing carburization temperature as is observed from the TEM images of the sample carburized at 1000°C, suggesting this constitutes the graphite layer reported in literature. This graphitic layer is proposed to provide the observed protection against bulk oxidation.

Graphitic carbon, amorphous carbon as well as molybdenum oxide are strong Raman scatterers [24]. Raman

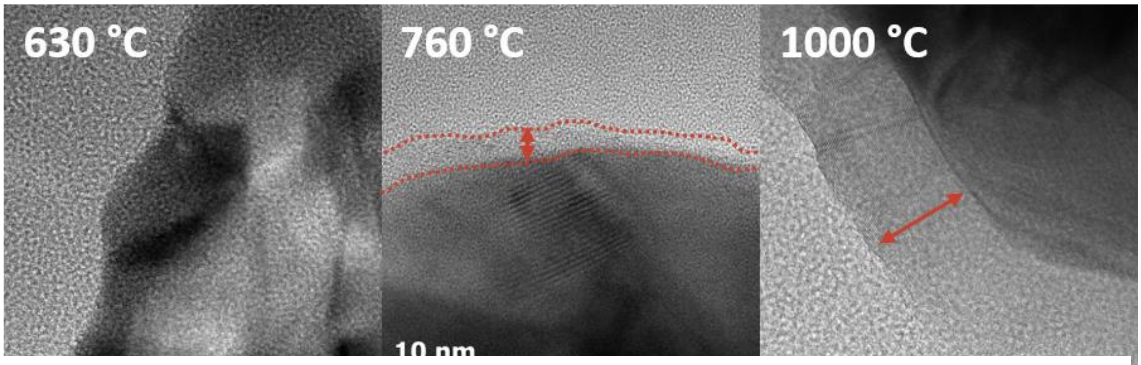

Fig. 2 TEM images of a particle from the samples carburized at 630, 760 and 1000 °C. At the temperature from 760 °C and above an unevenly distributed graphitic layer is observed on the edges of the particle, indicated by the dotted red lines and arrows.

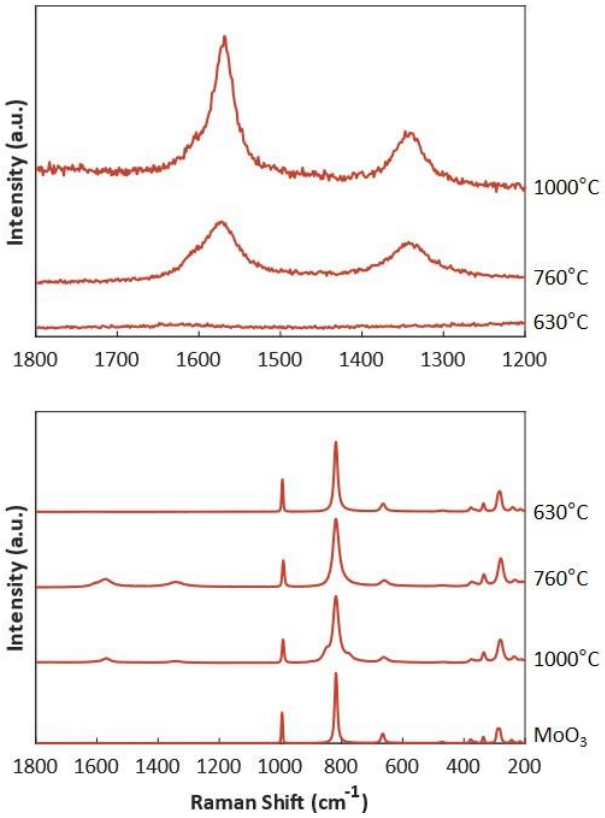

Fig. 3 Top figure: Raman spectra showing difference between D- and G-band intensities of the samples carburized at 630°C (no graphite visible), 760°C and 1000°C. Bottom figure: Raman spectra of samples carburized at 630°C, 760°C, 1000°C and MoO_3. All spectra show similar Raman spectra to MoO_3.

spectroscopy (Fig.3, top figure) of the samples confirmed that the observed layer in the TEM images is graphitic carbon, shown by the D- and G-band at approximately 1347 and 1588 cm^{-1}, respectively, with I_D/I_G ratios of 0.64 and 0.37 for the samples prepared at 760 and 1000°C (without passivation) confirming an increased graphitization with carburization temperature [32]. Interestingly, all samples show MoO_3 as well (Fig. 3, bottom figure). This indicates that, even though the bulk catalyst is β-Mo_2C, the surface is covered with a layer of MoO_3 after passivation and even in the absence of passivation.

While the carbon layer coating of the high temperature carburized samples prevents bulk oxidation after exposure to atmospheric air, it does not completely protect the β-Mo_2C. Possibly the diffusion of O_2 to the carbide surface is limited by the C-coating resulting in a mild passivation treatment, similar to the intentional passivation method, i.e. exposure to 1% O_2 in N_2 at room temperature.

Graphitic layer removal by temperature programmed hydrogenation. The surface structure of any catalyst is of course key to its performance. As it is proposed that the actual carbide phase is responsible for the desired catalytic activity, the samples carburized at 760˚C and 1000˚C, i.e. the samples covered by a graphitic carbon layer, were treated in a hydrogen stream to investigate the possibility of its removal. A temperature programmed hydrogenation (TPH) reaction was carried out inside the calcination unit (see Fig. S1 and S2). A significantly higher amount of CH_4 was formed, starting between 600-650°C, during the treatment of the 1000˚C carburized sample compared to the sample carburized at 760°C. This is in line with the thickness of the graphite layer observed in the TEM images and the intensity of the D- and G-band in the Raman spectra.

Consistent with the TEM images, Raman spectra, and TPH, the XPS analysis confirmed that the carbon content on the surface of the catalyst increased with increasing carburization temperature. After the hydrogen treatment, the absolute carbon content decreased and thus the oxygen content increased relatively (Fig. 4, left). Focusing just on the carbon content (Fig. 4, right) it was observed that at high carburization temperatures (≥760°C) the sample exhibits mainly graphitic carbon on the surface, increasing in concentration with temperature, consistent with all previous analysis. However, on the sample prepared at 630°C graphitic carbon was also detected, suggesting that carbon deposition already happens at temperatures as low as 630˚C, but not to such an extent that it

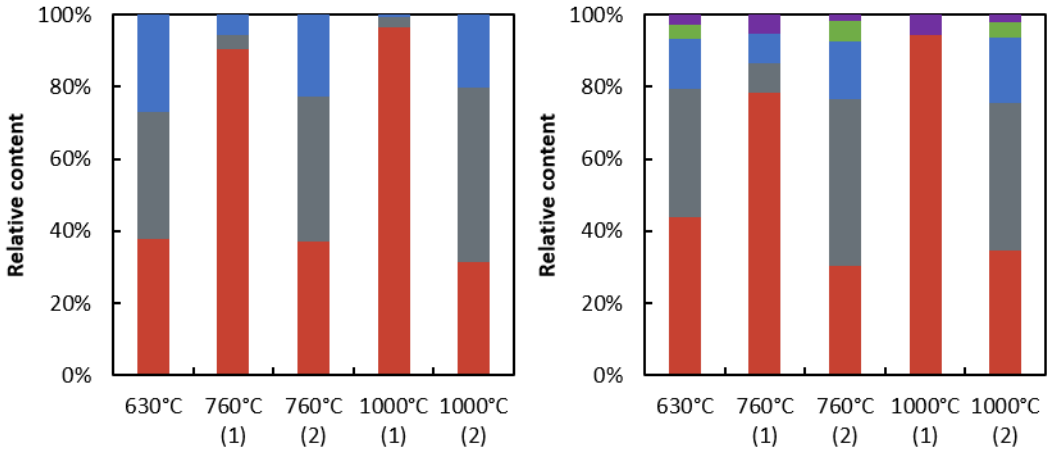

Fig. 4 XPS analysis of the samples carburized at 630, 760 and 1000°C before (1) and after (2) the TPH treatment. Figure on the left displays the C 1s (red), O 1s (grey) and Mo 3d (blue) relative content on the surface of the samples. Figure on the right displays the graphitic (red), carbidic (grey), C-O (blue), C=O (green) and saturated graphitic (purple) carbon relative content on the surface of the samples.

is visible in TEM or Raman analysis. The graphitic carbon, together with the carbidic carbon, makes up 80% of the carbonaceous composition on the surface of the catalyst. Other carbon phases that were observed include single and double bonded carbon to oxygen and saturated graphitic carbon. The temperature programmed hydrogenation of the samples prepared at ≥760°C decreased the graphitic phase, indicating that approximately 54-65% of the graphite layer is removed. Simultaneously, the single and double bonded oxygen to carbon compounds increased relatively. It is also observed that the ratios between the other carbon species (without the graphitic carbon) change upon the TPH treatment, which could indicate that not only graphitic carbon is removed. For example, for the 760°C sample the ratio between the carbide and the C-O is approximately 1, however, after TPH the ratio increased to approximately 3. This could indicate the removal of C-O species during the TPH treatment. After TPH treatment both the overall surface composition regarding C, O and Mo as well as the C speciation of the samples are comparable to the 630°C sample after carburization and passivation.

In situ XRD carburization of MoO_3 to β-Mo_2C. A sample was prepared and analysed *in situ* in the XRD at 650°C, passivated and subsequently reduced under hydrogen for 4.5 h at 400°C, as this condition was chosen for further FTS testing. After cooling down to room temperature, the sample was exposed to air. Offline XRD-analysis of the sample showed a small MoO_2 content (5.5 wt.%) which is suggested to be residual MoO_2 which failed to carburize, indicated by its small crystallite size of 12.7±1.4 nm and not the result of re-oxidation during the exposure to air. The carburization of the MoO_3 proceeds via the reduction to MoO_2 before yielding β-Mo_2C (Fig. 5), as is suggested by the method reported by Lee *et al.* (1987) [25]. Using Rietveld refinement techniques, the detailed bulk phase transitions can be elucidated in great detail, showing the initial reduction from MoO_3 to MoO_2 to start between 490-510°C yielding 99.9% MoO_2 at 640°C (Fig. 6, top). Carburization is first

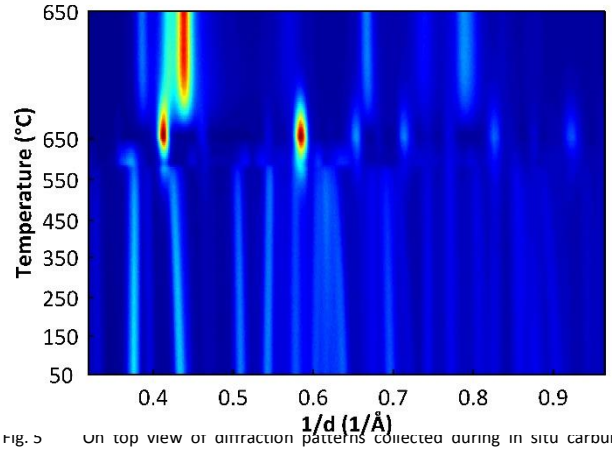

Fig. 5 On top view of diffraction patterns collected during in situ carburization experiment displaying phase transformation from MoO_3 to MoO_2 and finally β-Mo_2C. Conditions: T_{ramp} = 1°C/min, T_{final} = 650°C, SV = ±21 L/h/g_{cat}, carburization mixture: H_2 / CH_4 / N_2 = 9% / 2% / 89%, P = 1 atm, 1 scan per 5 min, total of 181 scans, step size 0.0287° and time per step is 0.2 s.

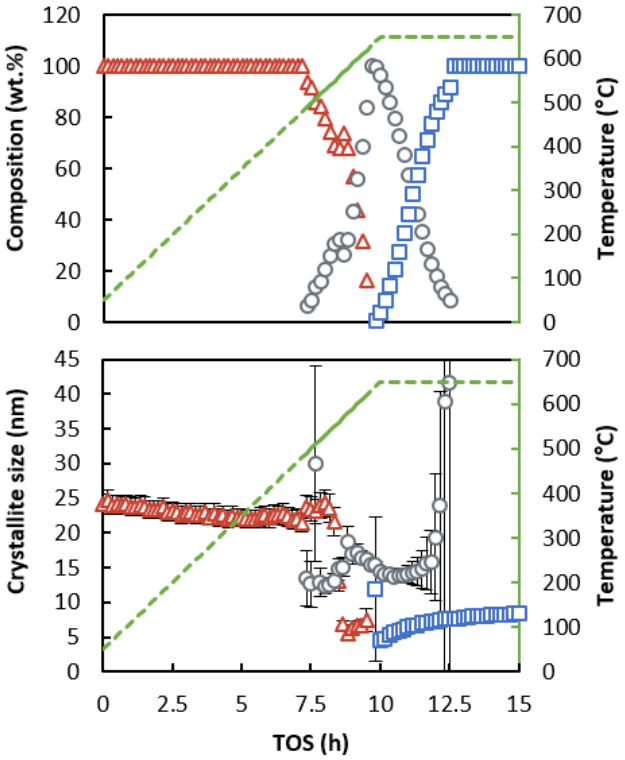

Fig. 6 Composition (top figure) and crystallite sizes (bottom figure) of the catalyst calculated using Rietveld refinement of the patterns collected in figure 5. Phases shown: MoO_3 (red triangles), MoO_2 (grey circles) and β-Mo_2C (blue squares). Note that error bars for most refinements are so small that they are covered by the data markers.

detected at 640°C, reaching a pure β-Mo_2C phase after 2.5 h at 650°C.

It should be noted that under *in situ* conditions no residual MoO_2 was detected. Only after the transfer to an offline XRD for higher resolution scans, the previously mentioned 5.5 wt.% MoO_2 were identified. As no residual MoO_2 was observed in samples carburized under the same conditions in a fixed bed reactor, even after passivation, it is hypothesised that the suboptimal hydrodynamic flow pattern of the *in situ* XRD cell, especially at the bottom of the bed, is responsible for the incomplete carburisation. Subsequent mixing of the sample during the preparation for offline XRD analysis exposes the MoO_2 phase.

The crystallite sizes of the different phases as a function of time on stream were determined (Fig. 6, bottom). During the initial heating, the crystallite size of MoO_3 decreases gradually from 25 nm to 21 nm. This could be associated to an artefact originating in the slight shift in position of some reflexes due to thermal expansion (Fig. 5) The reduced oxide phase (MoO_2) showed a decrease in size to approximately 15 nm, which is close to the theoretical predicted size reduction based on data from reference data files reported in the ICDD PDF_2 database. Initially β-Mo_2C is formed at about 5 nm increasing upon carburization to about 8.4 nm. This represents a larger decrease in crystallite size compared to MoO_2, than theoretically

expected, which could indicate crystallite brake-up during carburization.

Characterization of Fischer-Tropsch tested catalysts. All previous samples were prepared in the calcination unit. However, an *in situ* prepared catalyst will be discussed regarding its performance in the FTS. Thus, the catalyst needs to be carburized inside the reactor of the test unit under the same carburization conditions (630°C). XRD analysis (Fig. 7) confirmed a successful *in situ* synthesis, however, the catalyst showed much smaller crystallite sizes (average of 12 ± 0.1 nm) than the catalyst prepared in the calcination unit (average of 35 ± 0.3 nm). A possible reason for the larger crystallite sizes obtained in the calcination unit is an uneven isothermal zone resulting in temperature spikes or inferior hydrodynamic flow patterns resulting in local hotspots. Based on this finding, all catalysts prepared for the FT testing were prepared inside the testing unit for consistency regarding the preparation method and comparable crystallite sizes.

Three samples were prepared with potassium promotion; 6.2 wt.% (A), 5.4 wt.% (B) and 1.9 wt.% (C), analysed with ICP-OES to confirm the K/Mo loading (Table 1). For samples A and B, not sufficient amounts of sample were available to analyse before FT testing so only data from the spent catalyst (indicated by an asterisk) are given. The data for sample C before (1.9 wt.%) and after FT testing, C*, (1.8 wt.%) suggests that no significant loss of potassium is expected during FT reaction. In subsequent sections, the potassium promoted samples will all be referred to their loading quantified after FT testing.

Catalytic performance

Effect of carburization conditions on the activity and selectivity of the catalysts. Three bulk β-Mo_2C catalysts, prepared using different carburization conditions, were exposed to FTS-conditions. Two catalysts were prepared at 630°C, from which one was kept inside the reactor and one was passivated and subsequently reduced. A third catalyst was prepared at 760°C and subsequently exposed to the temperature programmed hydrogen treatment as was discussed. The CO-conversion was adjusted by changing reaction temperature and space velocity to allow for comparability at similar CO conversions and temperatures. All three catalysts produce mainly hydrocarbons (>0.71 HC ratio to total organic product, CO_2-free) with a rather small chain growth probability (≤0.41), in line with the observations from Ranhotra *et al.* (1987) [33]. A decrease in oxygenate formation was observed with an increase in CO conversion, especially for the 760°C carburized sample (0.29 to 0.08 OH ratio to total organic product, CO_2-free with a CO conversion from 12% to 45%, respectively). Within the oxygenated products, methanol was the most favourable product to be formed (≥66 C%) (Table 2).

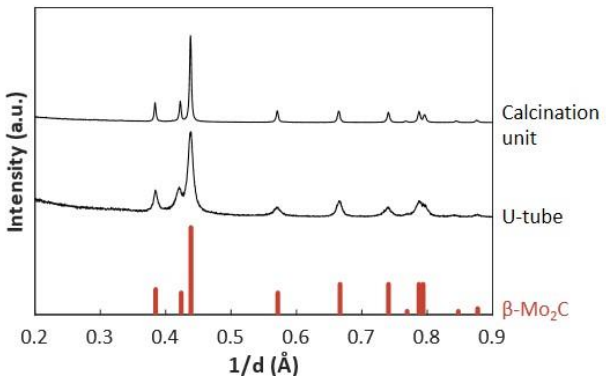

Fig. 7 XRD diffractograms of the two different samples prepared inside the calcination unit and the U-tube reactor.

Table 1 ICP-OES analysis results of the potassium promoted samples and an unpromoted sample.

Sample name	ICP-result wt.% K/Mo
Un-promoted	0.0%
A* - 6.2 wt.% K/Mo	6.2%
B* - 5.4 wt.% K/Mo	5.4%
C - 1.9 wt.% K/Mo	1.9%
C* - 1.8 wt.% K/Mo	1.8%

*spent sample, analyzed after FT

In addition to hydrogenation, all catalysts displayed a high activity for the WGS reaction, indicated by the high CO_2 selectivities (≥31 C%). The non-passivated catalyst showed highest CO conversion (85%), however, passivation of the catalyst is required for the promotion of the catalyst with potassium. Promotion of the catalyst prior to carburization (co-precipitation) has been reported by Kojima and Aika (2001) [34] and is reported to change the carburization process and enhance the formation of metallic molybdenum [22]. The sample undergoing a passivation/reduction treatment showed reduced CO conversion (maximum 55%) but at the same time, at very comparable conditions, an increased oxygenate selectivity (16 C% at 15% CO conversion, compared to 2% at 15% CO conversion for the *in situ* catalyst, both at 260°C). It also had the highest tendency to produce CO_2 (up to 53 C%), i.e. the

Table 2 FTS testing results on the samples prepared at 630°C (in situ and passivated) and at 760°C (after TPH treatment). Process conditions: P = 33 bar, H_2/CO ratio = 1. S = selectivity, HC = hydrocarbons, OH = oxygenates and CH3OH = methanol.

Catalyst	In situ		Passivated			760°C		
Space velocity (L/h/g_{cat})	16	16	16	9.6	9.6	12	8	8
Temperature (°C)	280	260	280	280	260	280	280	300
CO conversion	85%	15%	45%	55%	15%	9%	12%	45%
S CH_4[a]	37%	27%	24%	25%	20%	24%	21%	27%
S CO_2[a]	33%	31%	53%	45%	40%	31%	31%	41%
HC[b]	1.00	0.98	0.99	0.99	0.84	0.81	0.71	0.92
OH[b]	0.00	0.02	0.01	0.01	0.16	0.19	0.29	0.08
CH_3OH : Total OH	0.92	0.74	0.83	0.84	0.79	0.70	0.71	0.70
α_{3-8} paraffins	0.34	0.41	0.35	0.34	0.38	0.41	0.38	0.32
α_{3-8} olefins	n/a	0.30	0.23	0.24	0.27	0.30	0.28	0.28
α_{2-7} alcohols	n/a	0.17	n/a	n/a	0.14	0.16	0.15	0.19

[a]Carbon balance corrected (original value/total carbon balance)

[b]CO_2-free, ratio to total organic product (carbon based)

highest WGS activity, which might be related to residual MoO_x phases formed during passivation and retained after the mild reduction. Due to the high reduction temperature of MoO_x (Fig. 5), CO oxidation to CO_2 via a Mars van Krevelen type mechanism is unlikely.

Low temperature CO oxidation over MoO_3/CeO_2 has been reported and was suggested to follow either the Eley-Rideal or Langmuir-Hinshelwood mechanism [35]. However, these mechanisms require the presence of O_2 in the reactive gas mixture, which is not the case. The catalyst carburized at 760˚C exhibiting a graphite layer had, after TPH treatment, the lowest catalytic activity with a surprisingly high oxygenate selectivity – although a direct comparison of the catalytic performance is difficult and the stability of the catalyst regarding selectivity is uncertain. As addition of potassium to the catalyst has shown to negatively impact the catalytic activity [20] while significantly improving the oxygenate selectivity, the disadvantage of the lowered activity outweighs the possible selectivity advantages. Therefore, further detailed studies on catalyst activity and selectivity as function of reaction conditions and potassium loading were conducted with passivated and subsequently reduced catalysts under the same carburization conditions as the sample carburized at 630 °C.

Effect of potassium promotion on the activity and selectivity over β-Mo2C. The effect of potassium on the catalytic performance is significant. One of the observations, which is in line with reports in literature [20, 22], is that the CO conversion decreases upon promotion, however the amount of potassium, within the here studied boundaries, does not seem to influence the extent to which the catalytic activity decreases (Fig. 8, left). The unpromoted sample shows a CO conversion up to 34% at 300˚C, while samples A, B and C all show a CO conversion ≤10%, at the same reaction temperature and constant space velocity. The calculated activation energies show a drop with increasing potassium promotion from 122.4 kJ/mol for the unpromoted catalyst to 63.9, 54.9 and 40.8 kJ/mol with increasing potassium levels. Paralleled by the decrease in CO conversion, the selectivity to CH_4 decreases while the selectivity to CO_2 increases (Fig. 9).

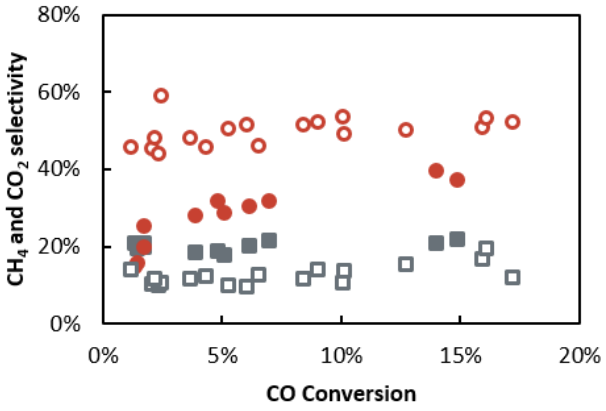

Fig. 9 Carbon balance corrected CH_4 (grey) and CO_2 (red) selectivities as a function of the CO conversion for the promoted samples (open symbols) and the unpromoted sample (solid symbols).

If both these C_1 product species (CH_4 and CO_2) are excluded from the amount of converted CO the conversions of the promoted samples at 300°C (approximately 5%) are very similar to the conversion of the unpromoted sample at 280°C (approximately 7%) (Fig. 8, right). This indicates that the higher CO conversions of the unpromoted samples are mainly higher due to their stronger tendency to produce CH_4 and CO_2. At these same points the oxygenate selectivity is significantly higher (approximately 21 C% vs 42 C%, CO_2-free and 32 C% vs 58 C%, CO_2- and CH_4-free) for the promoted samples.

Besides the effect on the activity, WGS and chain growth, potassium promotion has also shown to have a significant effect on the product selectivity. Where the unpromoted sample does not show a linear olefin to linear paraffin (exemplary for C_3) ratio of higher than 1.26 at very low conversions (±1%), the promoted samples lowest observed linear olefin to linear paraffin ratio is 2.43 at a similar CO conversion. The higher the CO conversion, the lower the linear olefin to linear paraffin ratio

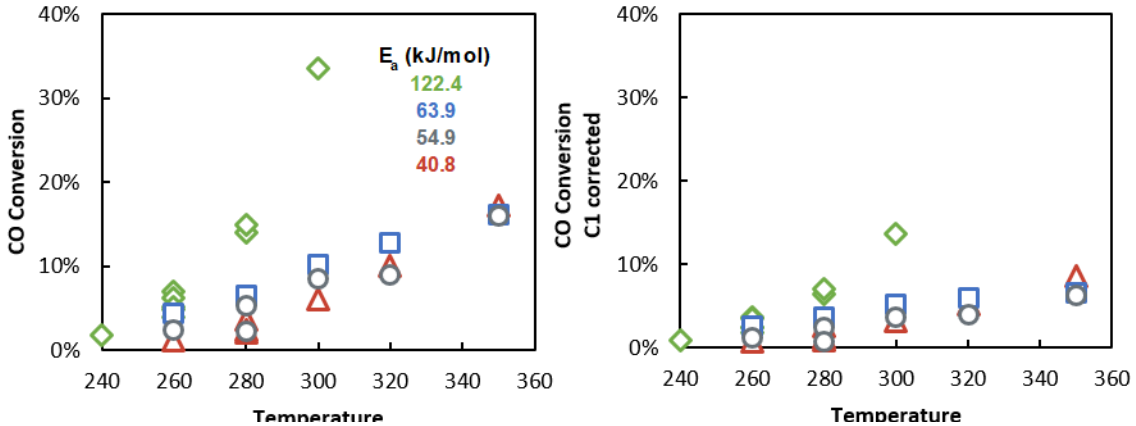

Fig. 8 Effect of potassium promotion and temperature on the original (figure on the left) and the C1-corrected – without CH_4 and CO_2 - (figure on the right) CO conversion over β-Mo_2C. The following samples are shown: A (red triangles), B (grey circles), C (blue squares) and the unpromoted sample (green diamonds). Letters A to C refer to K loading levels as introduced in table 1.

for the unpromoted sample (Fig. 10). However, this trend does not hold for the promoted samples. The hypothesized suppression of secondary hydrogenation reactions commonly described as the mechanism of potassium promotion, yielding higher olefin contents [36] does not seem to be influenced by conversion levels nor reaction temperature.

The chain growth probability is a good handle to explain the chance to form longer chained products. An ASF-distribution can be defined for each group of products per sample, and from these plots a certain α-value can be calculated, indicating the chain growth probability. The α-values calculated for the linear olefins (based on carbon numbers C_3-C_8) are between 0.42 and 0.53 for the promoted samples, and for the unpromoted samples between 0.32 and 0.23. Besides the reported intrinsic increase in chain growth induced by potassium promotion, the hydrogenation activity of the unpromoted sample is expected to be higher causing more secondary hydrogenation of primarily formed olefins. Interestingly, the chain growth probability remains relatively constant over all levels of CO conversion (see Fig. S3). The effect of potassium promotion on the chain growth of linear paraffins is lower, with only a small increase in the chain growth probability. Again, the more pronounced secondary hydrogenation of the olefin products over the unpromoted sample does increase the overall paraffin selectivity balancing in part the expected performance benefit of the promotion. A slight increase in α-values with a decreasing CO conversion is measured (see Fig. S4).

The focus of the present study is the formation of oxygenates which was reported to be enhanced by potassium promotion [20, 22, 23, 29, 37]. Due to the high CO_2 selectivities, it is of interest to compare the formation towards oxygenates and hydrocarbons without CO_2. The total oxygenate yield, calculated on a CO_2-free basis, is plotted against the CO conversion towards organic products (thus without CO_2) in order to compare the oxygenate production of the promoted samples with the unpromoted sample. It is observed that at higher CO conversions, the promoted samples show significant higher oxygenate selectivity compared to the unpromoted sample (Fig. 11). This could be the result of secondary formation

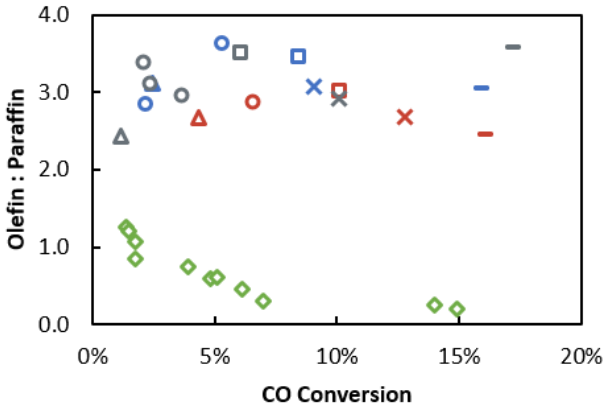

Fig. 10 C_3-linear olefin to C_3-linear paraffin ratio of samples A (grey), B (blue), C (red) and the unpromoted sample (green diamonds) are shown at varying temperatures of 260°C (triangles), 280°C (circles), 300°C (squares), 320°C (crosses) and 350°C (dashes).

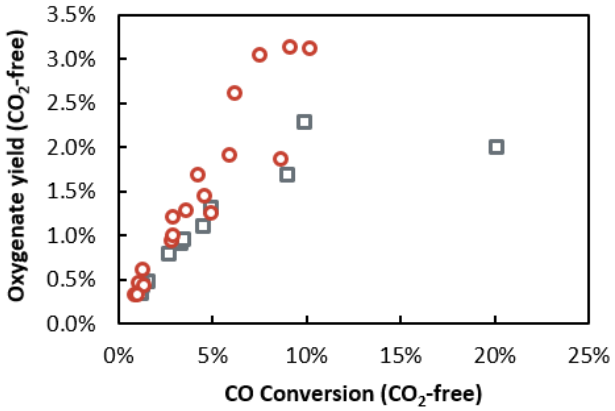

Fig. 11 Oxygenate yield (CO_2-free) of the promoted samples (red circles) compared to the unpromoted sample (grey squares).

routes or in fact the suppression of secondary reactions (hydrogenation) resulting in the loss of the oxygenate functionality over potassium promoted catalysts.

While in the absence of potassium the alcohol fraction remains constant with increasing conversion, the promoted samples produce a significant number of aldehydes (up to 37 C% at 2% CO conversion), specifically at lower CO conversions. Small traces of ketones and carboxylic acids are formed (together ±10 C% at low CO conversions <5%). Aldehydes and carboxylic acids might represent fractions of the primary oxygenate product. However, over the unpromoted catalyst, these are hydrogenated in secondary reactions to alcohols or indeed paraffins. With increasing conversion, the content of aldehydes, ketones and carboxylic acids decreases and the oxygenate product stream is dominated by alcohols (Fig. 12).

Within the oxygenate fraction, the unpromoted samples have shown to form mainly methanol, up to a methanol to total oxygenate ratio of 0.92 at 85% CO conversion and a lowest ratio of 0.49 at 2% CO conversion. The promoted samples don't show a higher ratio than 0.32 which indicates that higher alcohols are more favourable to be formed upon promotion with potassium (Fig. 13).

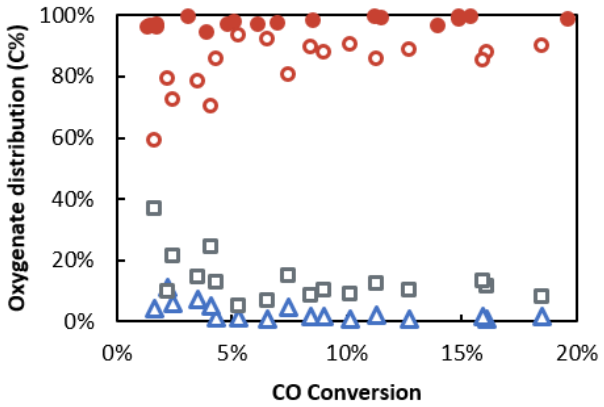

Fig. 12 Distribution of the different product classes within the oxygenated compounds, comparison between promoted (open symbols) and unpromoted (solid symbols) samples, with alcohols (red circles), aldehydes (grey squares) and other oxygenated products such as ketones and carboxylic acids (blue triangles).

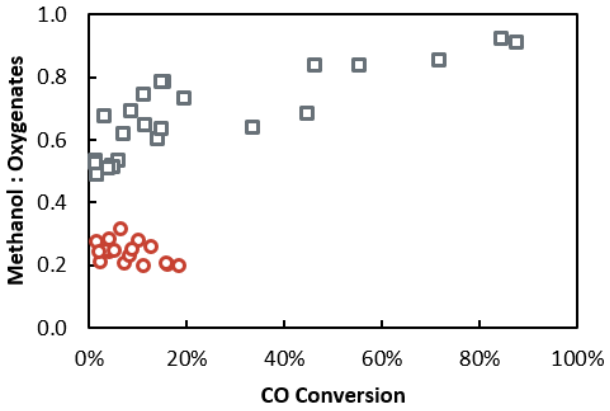

Fig. 13 Methanol to oxygenate ratio of the promoted samples (red circles) and the unpromoted samples (grey squares).

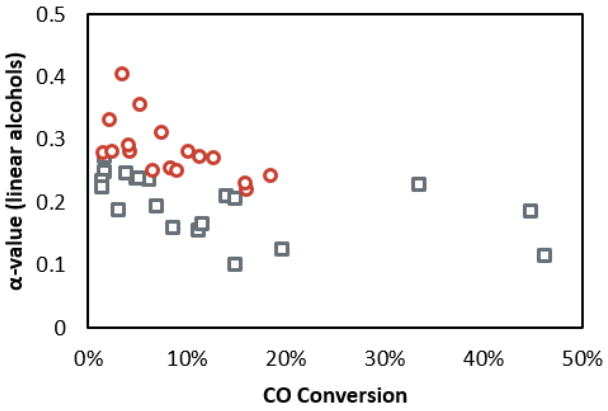

Fig. 14 Chain growth probability as a function of CO conversion towards linear alcohols for promoted (red circles) and unpromoted (grey squares) samples.

The chain growth probability of linear alcohols (based on carbon numbers >C_2) confirms this observation upon addition of potassium. However, the chain growth probability is still rather low, with a maximum measured chain growth probability around 0.4. This indicates that, even though it was observed that the methanol formation significantly decreases, the main alcohol products have chain lengths with carbon numbers between C_2-C_4 (Fig. 14). The promoted samples produce predominantly ethanol (up to 54 C%). It is observed that with an increase in CO conversion, the methanol content decreases, where ethanol and propanol increases (Fig. 15). At the higher conversions, the selectivity towards methanol and propanol are almost equal. However, due to the domination of ethanol, the chain growth probability remains relatively low.

Conclusions

This study presents the effect of synthesis protocols and potassium promotion on a β-Mo_2C catalyst in the oxygenate formation during the Fischer-Tropsch synthesis.

The graphitic carbon layer, formed during high temperature carburization (≥760°C), can be partially removed by means of a TPH reaction, forming CH_4. The bulk carbide catalyst remained stable in air, which confirms that there is no bare carbide surface.

In situ XRD analysis of the carburization of MoO_3 confirmed that phase transformation to β-Mo_2C happens at 650°C. Partial oxidation to MoO_2 was observed after exposure to air without a passivation treatment.

Raman analysis of all samples - after exposure to air – showed MoO_3 spectra despite the carburization method used. The catalyst carburized *in situ* at 630°C showed higher CO hydrogenation activity than the passivated and subsequently reduced catalyst, at the same carburization temperature. The high temperature carburization, 760°C showed that the carbon deposition in the form of graphite significantly affects the activity of the catalyst, even after TPH treatment.

The passivated sample showed higher oxygenate to total organic product ratios than the *in situ* prepared sample at similar conversion levels, which has not been reported before. It is suggested that the presence of MoO_3 on the surface of the catalyst influences the formation of oxygenates, which was for unpromoted catalysts mainly methanol. Additionally, a higher activity for the WGS was observed for the passivated samples.

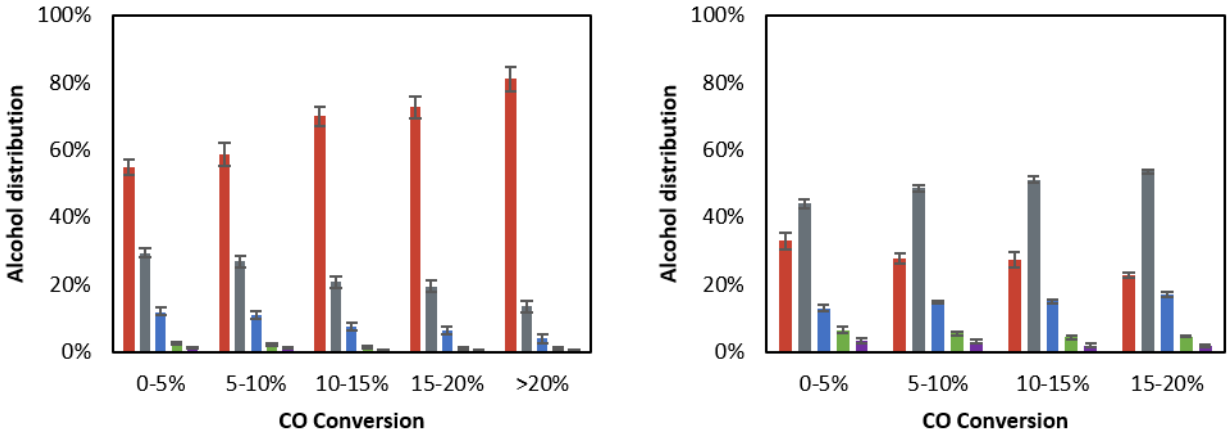

Fig. 15 Alcohol distribution over the unpromoted samples (figure on the left) and the promoted samples (figure on the right) as a function of the CO conversion, with from left to right per series methanol (red, #1), ethanol (grey, #2), propanol (blue, #3), C4 alcohols (green, #4) and C5+ alcohols (purple, #5).

Potassium promotion increased oxygenate selectivity at all applied process conditions, compared to the unpromoted samples. However, the difference in promotion levels did not show a significant effect regarding activity and selectivity.

An increase in higher oxygenates (C_{2+}) was observed for the potassium promoted samples, especially ethanol in comparison to methanol. Increasing reaction temperature leads to a decrease in the methanol content, while increasing the ethanol selectivity. However, the increase in temperature also enhances the formation of hydrocarbons, lowering the total selectivity towards oxygenates. This effect is more pronounced in the case of the unpromoted sample which could be explained by a secondary formation route of oxygenates over the promoted catalyst or rather via the suppression of the secondary hydrogenation of oxygenates to paraffins by potassium. Formation of aldehydes, ketones and carboxylic acids were also observed, which are significantly reduced by an increase in temperature/CO conversion. This again points towards a suppressed secondary hydrogenation activity of the promoted sample. In the unpromoted catalyst aldehydes and carboxylic acids formed could be directly hydrogenated to the corresponding alcohol or paraffin.

Conflicts of interest

There are no conflicts to declare.

Acknowledgements

The authors would like to thank c*change (DST-NRF Centre of Excellence in Catalysis), the Newton Fund and the Royal Society in form of the Newton Advanced Fellowship program, the Catalysis Institute at the Department of Chemical Engineering, University of Cape Town for their financial and experimental support. The help from Prof Patricia Kooyman for her assistance with the TEM analysis, Zulfa le Riche and Stephanie la Grange for ICP-OES analysis, Dr Hendrik Kotzé and Dr Mohamed Fadlalla from the University of Cape Town is much appreciated.

Notes and references

1 F. Fischer, Industrial & Engineering Chemistry, 1925, **17**, *6*, 574-576.
2 F. Fischer, National Petroleum News, 1926, **18**, 49.
3 F. Fischer and H. Tropsch, Brennstoff-Chemie, 1926, **7**, 299-300.
4 F. Fischer and H. Tropsch, Brennstoff-Chemie, 1926, **7**, 97-104.
5 F. Fischer and H. Tropsch, Brennstoff-Chemie, 1928, **9**, 39.
6 H. Schulz, Applied Catalysis A: General, 1999, **186**, 3-12.
7 R. D. Entenberg and A. L. Menard. Jr., Journal of Marketing, 1966, **30**, 28-32.
8 A. Marin and D. Kodjak, "Relative Cancer Risk of Reformulated Gasoline and Conventional Gasoline Sold in the Northeast," Northeast States for Coordinated Air Use Management, Boston, USA1998.
9 J. Stolark, "Fact Sheet - a Brief History of Octane in Gasolinel from Lead to Ethanol," Environmental and Energy Study Institute2016, Available: http://www.eesi.org/papers/view/fact-sheet-a-brief-history-of-octane.
10 V. R. Surisetty, A. K. Dalai, and J. Kozinski, Applied Catalysis A: General, 2011, **404**, *1-2*, 1-11.
11 A. d. Klerk, Energy & Environmental Science, 2011, **4**, *4*, 1177.
12 P. Courty, D. Durand, A. Sugier, and E. Freund, Process for Manufacturing a Mixture of Methanol and Higher Alcohols from Synthesis Gas, France Patent 4,659,742, 1987.
13 N. D. Subramanian, G. Balaji, C. S. S. R. Kumar, and J. J. Spivey, Catalysis Today, 2009, **147**, *2*, 100-106.
14 X. Zhang, Z. Li, Q. Guo, H. Zheng, and K. Xie, Fuel Processing Technology, 2010, **91**, *4*, 379-382.
15 D. Mahajan and P. Vijayaraghava, Fuel, 1999, **78**, 93-100.
16 M. Pijolat and V. Perrichon, Applied Catalysis, 1985, **13**, 321-333.
17 P. Forzatti, E. Tronconi, and I. Pasquon, Catalysis Reviews - Science and Engineering, 1991, **33**, 109-168.
18 S. T. Oyama, Catalysis Today, 1992, **15**, 179-200.
19 S. F. Zaman, N. Pasupulety, A. A. Al-Zahrani, M. A. Daous, S. S. Al-Shahrani, H. Driss, L. A. Petrov, and K. J. Smith, Applied Catalysis A: General, 2017, **532**, 133-145.
20 H. C. Woo, K. Y. Park, Y. G. Kim, I. Nam, J. S. Chung, and J. S. Lee, Applied Catalysis, 1991, **75**, 267-280.
21 M. L. Xiang, D. B. Li, H. C. Xiao, Z. L. Hanli, H. J. Qi, W. H. Li, B. Zhong, and Y. H. Sun, Fuel, 2008, **87**, *4-5*, 599-603.
22 M. L. Xiang, D. B. Li, W. H. Li, B. Zhong, and Y. H. Sun, Fuel, 2006, **85**, *17-18*, 2662-2665.
23 Q. X. Wu, J. M. Christensen, G. L. Chiarello, L. D. L. Duchstein, J. B. Wagner, B. Temel, J. D. Grunwaldt, and A. D. Jensen, Catalysis Today, 2013, **215**, 162-168.
24 T. Mo, J. Xu, Y. Yang, and Y. W. Li, Catalysis Today, 2016, **261**, 101-115.
25 J. S. Lee, S. T. Oyama, and M. Boudart, Journal of Catalysis, 1987, **106**, 125-133.
26 D. V. N. Vo and A. A. Adesina, Applied Catalysis a-General, 2011, **399**, *1-2*, 221-232.
27 Z. Yin, Q. Zhao, S. Chen, G. Liu, and S. Wang, Journal CSIMM, 1993, **24**, *4*, 541-546.
28 S. W. Chiang, C. C. Chang, J. L. Shie, C. Y. Chang, D. R. Ji, and J. Y. Tseng, Journal of the Taiwan Institute of Chemical Engineers, 2012, **43**, *6*, 918-925.
29 J. M. Christensen, L. D. L. Duchstein, J. B. Wagner, P. A. Jensen, B. Temel, and A. D. Jensen, Industrial & Engineering Chemistry Research, 2012, **51**, *11*, 4161-4172.
30 J. Patt, D. J. Moon, C. Phillips, and L. Thompson, Catalysis Letters, 2000, **65**, 193-195.
31 H. M. Rietveld, Journal of Applied Crystallography, 1969, **2**, 65-71.
32 D. S. Knight and W. B. White, Journal of Materials Research, 1989, **4**, *02*, 385-393.
33 G. S. Ranhotra, A. T. Bell, and J. A. Reimer, Journal of Catalysis, 1987, **108**, 40-49.
34 R. Kojima and K. Aika, Applied Catalysis A: General, 2001, **219**, 141-147.
35 M. M. Mohamed and S. M. A. Katib, Applied Catalysis A: General, 2005, **287**, *2*, 236-243.
36 H. F. Xiong, M. A. Motchelaho, M. Moyo, L. L. Jewell, and N. J. Coville, Fuel, 2015, **150**, 687-696.
37 E. T. Liakakou and E. Heracleous, Catalysis Science & Technology, 2016, **6**, *4*, 1106-1119.